IEEE Photonics Journal
An IEEE Photonics Society Publication

Open Access

A Miniature Endoscopic Optical Coherence Tomography Probe Based on C-Lens

Volume 10, Number 5, September 2018

Site Luo
Liang Zhou
Donglin Wang
Can Duan
Hao Liu
Yu Zhu
Guoxin Li
Hui Zhao
Jianyu Tang
Yuqing Wu
Xin An
Xinling Li
Yabing Liu
Huikai Xie
Li Huo

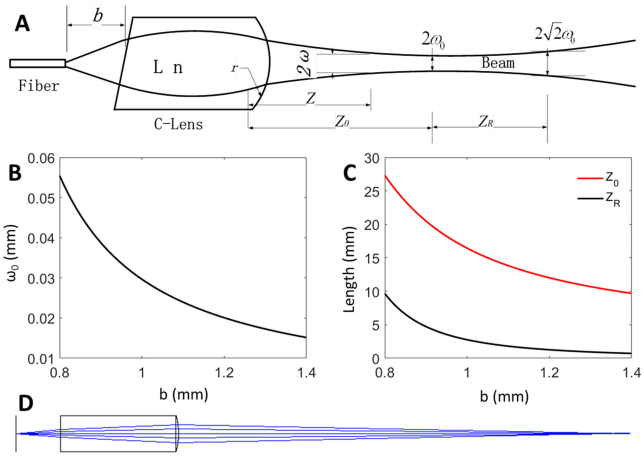

DOI: 10.1109/JPHOT.2018.2870690

A Miniature Endoscopic Optical Coherence Tomography Probe Based on C-Lens

Site Luo,[1,8] Liang Zhou,[2] Donglin Wang,[3,4] Can Duan,[2] Hao Liu,[5] Yu Zhu,[5] Guoxin Li,[5] Hui Zhao,[6] Jianyu Tang,[1] Yuqing Wu,[7] Xin An,[7] Xinling Li,[4] Yabing Liu,[4] Huikai Xie,[2,4] and Li Huo[1]

[1]Department of Electronic Engineering, Tsinghua University, Beijing 100084, China
[2]University of Florida, Gainesville, FL 32611-613 USA
[3]School of Physics and Electronic Engineering, Zhengzhou University of Light Industry, Zhengzhou 450000, China
[4]Wuxi WiO Technologies Co., Ltd., Wuxi 214000, China
[5]Department of General Surgery, Nanfang Hospital, Southern Medical University, Guangzhou 510515, China
[6]Foshan Optomedic Technologies Co., Ltd., Foshan 280000, China
[7]Suzhou Institute of Nano-Tech and Nano-Bionics, Chinese Academy of Sciences, Suzhou 215000, China
[8]Shenzhen Institutes of Advanced Technology, Chinese Academy of Sciences, Shenzhen 518000, China

DOI:10.1109/JPHOT.2018.2870690

Manuscript received July 11, 2018; revised September 11, 2018; accepted September 12, 2018. Date of publication October 5, 2018; date of current version October 10, 2018. This work was supported in part by the National Natural Science Foundation of China (No. 61575107, No. 61528401), in part by the State's Key Project of Research and Development Plan (2017YFC0108301), and in part by the U.S. National Science Foundation under Award#1512531. Corresponding authors: Huikai Xie and Li Huo (email: hkx@ufl.edu; lhuo@mail.tsinghua.edu.cn).

Abstract: We present a novel miniature endoscopic optical coherence tomography (OCT) probe based on an electrothermal microelectromechanical (MEMS) mirror and a C-lens. The MEMS mirror has a relatively large mirror plate of 0.5 mm × 0.5 mm on a small chip size of 1.5 mm × 1.3 mm, leading to the outer diameter of the endoscopic probe down to only 2.5 mm so that the probe is capable of being inserted through the biopsy channel of a conventional endoscope. A long focal length of 12 mm is achieved by properly designing the C-lens. Compared to commonly used GRIN lenses, C-lenses have advantages of much smaller sensitivities of the working distance and spot size to machining variations. The C-lens based probe can scan a large field of view (FOV) of 6 mm × 6 mm at only 5-V drive voltage. A swept source endoscopic OCT system is constructed using this miniature probe. Experiments show that the corresponding lateral and axial resolutions are about 50 and 14 μm, respectively. Various samples including human fingers, onions, and cancerous colon tissue are imaged and the result suggests this large-working-distance, large-FOV endoscopic probe is promising for applications in large tubular organs and large-area lesions.

Index Terms: Swept-source optical coherence tomography, endoscopic imaging, micro-optics.

1. Introduction

A large number of optical coherence tomography (OCT) endoscopic probes have been demonstrated in the past two decades and their optical scanning modes mainly include forward scanning, side scanning and circumferential scanning [1]. The circumferential scanning was first reported in 1997 [2], which is utilized extensively now for OCT imaging within hollow organs, such as artery, esophagus, and colon [2]–[4]. Circumferential scanning can be obtained by proximally driving an optical assembly using a torque cable or by distally rotating a prism to scan the light beam in the direction perpendicular to the axis of the imaging probe [5]–[8]. The side scanning is usually based on gradient-index (GRIN) lenses and MEMS scanning mirrors to achieve two-dimensional (2D) optical scans and three-dimensional (3D) OCT images [9], [10]. For an endoscopic OCT probe, the diameter, working distance and lateral resolution are the key parameters. In a MEMS OCT probe, a GRIN lens is often used to match the optical fiber and minimize the diameter of the probe and simplify the assembly, and the MEMS mirror typically scans an angular FOV of about 10°–20° [9]–[12]. Jung *et al.* employed a 2-axis scanning MEMS mirror to realize a 1 mm^2 scanning area [11]. Kim *et al.* reported a probe with a large optical scan angle of 40°, but still only imaged an area of approximately 3 mm^2 [13]. Sun *et al.* and Wang *et al.* respectively demonstrated 3-D endoscopic OCT imaging with a two-axis MEMS scanning mirror and the imaging areas were about 4 mm^2 [12], [14]. Duan *et al.* further improved the OCT imaging area up to 5 mm^2 [15].

In the case of applying OCT to large tubular organs, such as esophagus, where the diameter of the lumen is in the order of 20–25 mm. A technology based on a thin fiber-prism assembly spinning in a balloon has been exploited for esophagus OCT imaging [16]. This technology provides full 360°FOV and is very efficient to acquire circumferential images, but it has difficulty to image a localized specific region of interest. For instance, during OCT imaging of an esophagus, the physician might want to scan a highly suspecious area repeatedly in real time instead of analyzing the whole 3D esophagus image after reconstruction. Besides, some cancers may appear in a large flat area instead of a tubular organ, such as stomach cancer, cervical cancer and oral cancer, which are not applicable for circumferential scanning probes [17]–[20]. MEMS based OCT would be a good alternative, but as described above, almost all of the MEMS OCT probes reported are based on GRIN lenses and typically have small imaging areas due to small working distances [11], [12], [14], [15]. The working distances of these MEMS OCT probes are mainly limited by the available pitches (i.e., 023, 0.25 or 0.27) of commercial GRIN lenses. Duan *et al.* did an extensive study showing that the maximum working distance of GRIN lenses at 0.27 pitches is less than 6.0 mm [21]. Suter *et al.* and Kang *et al.* reported long-focal-length OCT probes based on GRIN lenses, respectively [22], [23]. Fu *et al.* reported an OCT imaging catheter with a 9-mm working distance utilizing a glass rod and two GRIN lenses [24]. Xi *et al.* reported an OCT probe with an 11-mm working distance by cutting and fine polishing one GRIN lens down to 0.05-pitches [25]. Numerical simulation has shown that GRIN lenses must be extremely short and machined with ultra-high precision, which drastically increases the cost and the lead time [26], [27]. On the other hand, C-lenses are also rod lenses and can achieve long working distance; more importantly, C-lens collimators are available off the shelf and have been widely used in optical communications [29]–[31]. Therefore, we propose to use a C-lens in a MEMS OCT probe to increase the working distance and thus increase the imaging area. Another advantages of using C-lenses is that a C-lens' sensitivities of the working distance and spot size to its length are much lower than those of a GRIN lens.

In this study, a detailed analysis of using C-lenses for obtaining long focal length is performed, and a comparison to GRIN lenses is also made. To validate this C-lens based method, a miniature endoscopic probe using a C-lens has been designed, assembled and tested. The probe has an outer diameter of only 2.5 mm and the rigid length is 8.5 mm so that it can be directly inserted through the biopsy channels of most of conventional endoscopes for noninvasive in vivo imaging. The small probe diameter is enabled by the high fill factor of a unique electrothermal MEMS mirror. In the following, we will first introduce the optical and mechanical design of the C-lens based MEMS

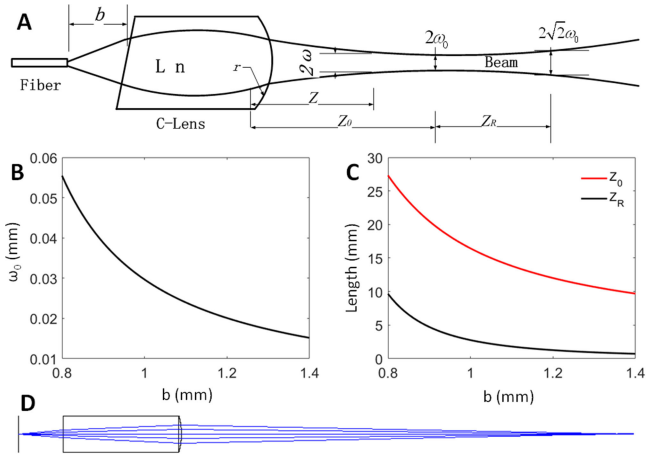

Fig. 1. (A) The optical schematic diagram of the C-lens collimator. (B) The plot of w_0, over b. (C) The plots of Z_0 and Z_R and over b. (D) The Zemax simulation schematic diagram.

OCT probe, and then we compare the sensitivity of the working distance and spot size to the dimensional variations or machining errors of the GRIN lens and C-lens. Finally we report the test experiments and present the OCT imaging results using the new probe.

2. Methods

A C-lens is a rod lens with a uniform refractive index and a spherical surface at its rear end, and C-lenses can be used to achieve long working distance [29]. Compared with GRIN-lens, C-lens features with low cost and easy control of lens' parameters. The optical model of a C-lens collimator consisting of a C-lens and a single-mode fiber is shown in Fig. 1(A). The distance between the fiber end and the C-lens front end is defined as b, and this space is filled with air. The output beam from the C-lens rear end is considered as a Gaussian beam. The beam waist w_0, waist position Z_0 and Rayleigh range Z_R of the output beam can be calculated using the ABCD matrix method and are determined by the diameter, d, length, L, radius of curvature, r, and refractive index, n, of the C-lens and b. Note that both the fiber end and the C-lens front end are cut with an 8° angle to minimize back reflection. The ABCD matrix of the C-lens is expressed as:

$$T = \begin{bmatrix} 1 & 0 \\ \frac{n_0-n}{n_0 r} & \frac{n}{n_0} \end{bmatrix} \begin{bmatrix} 1 & L \\ 0 & 1 \end{bmatrix} \begin{bmatrix} 1 & 0 \\ 0 & \frac{n_0}{n} \end{bmatrix} = \begin{bmatrix} 1 & L\frac{n}{n_0} \\ \frac{n_0-n}{n_0 r} & \left[\frac{n_0-n}{n_0 r}L + \frac{n}{n_0}\right]\frac{n_0}{n} \end{bmatrix} \tag{1}$$

The ABCD matrix at a position Z can be calculated as:

$$M = \begin{bmatrix} A & B \\ C & D \end{bmatrix} = \begin{bmatrix} 1 & z \\ 0 & 1 \end{bmatrix} T \begin{bmatrix} 1 & b \\ 0 & 1 \end{bmatrix} \tag{2}$$

Using Eqs. (1) and (2) with multiple iterations, the C-lens' parameters are selected as $d = 1$ mm, $L = 3.2$ mm, $r = 1.8$ mm, and $n = 1.74$. Then the calculated w_0, and Z_0/Z_R over b are shown in Figs. 1(B) and 1(C), respectively. The design of the C-lens-based collimator is optimized using Zemax. Based on the data in Figs. 1(B) and 1(C), b and the beam waist are set as 1.2 mm and 12 mm, respectively, resulting in the spot diameter of the beam waist of about 45 μm and the depth of focus of 2.2 mm. This result is verified by Zemax simulation as shown in Fig. 1(D). Note that the 8° cut is not included in the Zemax model for simplicity. Also note that the parameters of the fabricated probe will be slightly deviated from the theoretical calculation due to the unavoidable manufacturing errors, and the test result of the actual probe will be shown in Fig. 4.

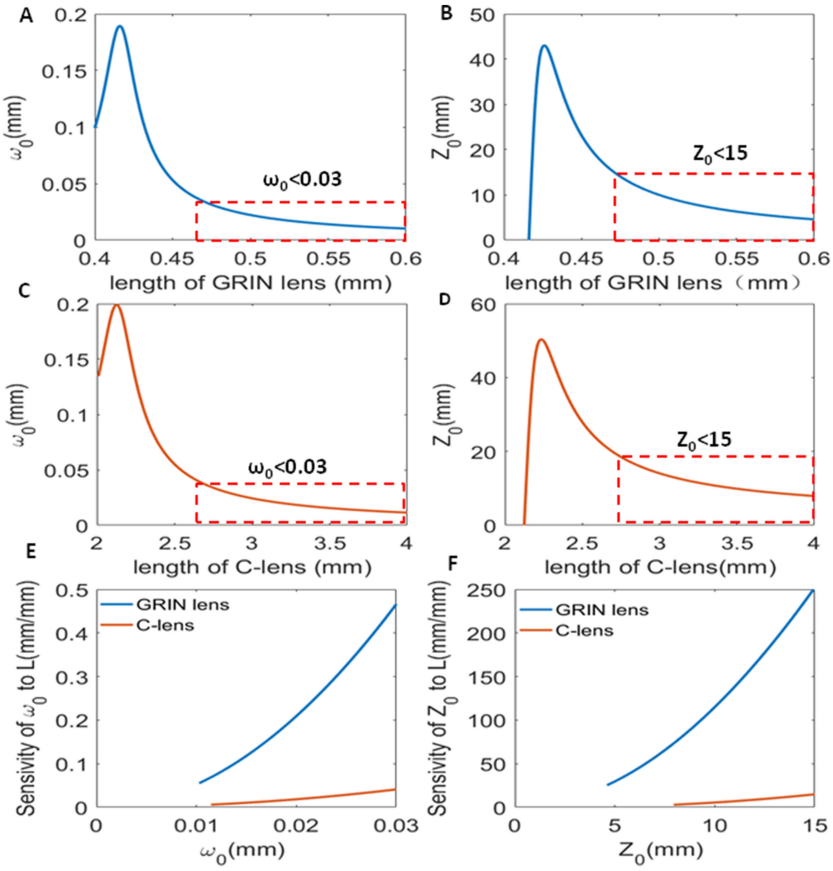

Fig. 2. Comparison of C-lens to GRIN lens. A: the spot radius versus the GRIN lens length. B: the working distance versus the GRIN lens length. C: the spot radius versus the C-lens length. D: the working distance versus the C-lens length. E: the sensitivity of the spot radius to the lengths of the GRIN lens and C-lens. F: the sensitivity of the working distance to the lengths of the GRIN lens and C-lens.

The dependence of the designed parameters on the manufacturing precision determines the cost and lead time of those components. W. Jung *et al.* demonstrated the relationship between the working distances, beam width and pitch number of a GRIN lens, and they also reported a method for designing long-working-distance probes [27]. This work shows that a working distance in the range of 9–14 mm can be obtained with an extremely short pitch number (0.04–0.045), but the working distance is very sensitive to the pitch number, and a 0.001 pitch variation will result in a change of the working distance by 1 mm and a change of the spot size by 2 μm [27].

A comparison between a GRIN lens and a C-lens regarding the focal length and spot size and their sensitivities to the lens length is shown in Fig. 2. The length of the GRIN lens and the C-lens are set at different ranges to ensure similar working distances and beam widths. In this comparison, the parameters of the GRIN lens are set as follows: n = 1.6164, g = 0.8521 mm^{-1}, b = 1.95, and L = 0.4–0.6 mm. The parameters of the C-lens are: n = 1.74, r = –1.8 mm, b = 1.20, and L = 2.0–4.0 mm. Figs. 2(A, B) and 2(C, D) show the spot radii and working distances at various L's of the GRIN lens and the C-lens, respectively. The red dashed line boxes in Figs. 2(A) and 2(C) correspond to the spot radius range of interest of $\omega_0 < 0.03$ mm while the red dashed boxes in Figs. 2(B) and 2(D) correspond to $Z_0 < 15$ mm. Fig. 2(E) shows the sensitivities of the spot radius to L at the length range of interest of the GRIN lens and C-lens, where the x axis is labelled with ω_0 by changing L to the corresponding spot radius. The sensitivities are basically the slopes of the

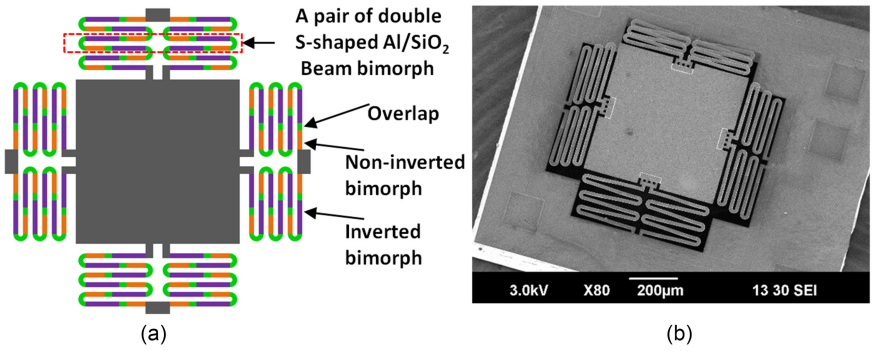

Fig. 3. (a) Top view of a MEMS Mirror design. (b) An SEM image of the MEMS mirror.

lines in Figs. 2(A) and 2(C). Similarly, Fig. 2(F) shows the sensitivities of the working distance to L at the range of interest.

As shown in Fig. 2(E), the sensitivity of ω_0 to L of the GRIN lens is 0.207 mm/mm at $\omega_0 =$ 0.02 mm, which means that the longitudinal tolerance of the GRIN lens should be about 5 μm to keep the variation of ω_0 within 1 μm. In contrast, for the C-lens, the sensitivity is 0.018 mm/mm, about 10 ten times less than that of the GRIN lens, so the tolerance can be extended to 55 μm to ensure the same variation of ω_0. As shown in Fig. 2(F), the sensitivity of Z_0 to L of the GRIN lens is 24 times as much as that of the C-lens. The sensitivity of the C-lens is 5 mm/mm at $Z_0 = 10$ mm, which means that the longitudinal tolerance of the C-lens is 200 μm to keep the variation of Z_0 within 1 mm. In contrast, a much smaller tolerance (down to 8.3 μm) is required for the GRIN lens. For precision machining, tolerance of several micrometers is much more expensive than that of hundreds of micrometers. Thereby, C-lenses are a better choice for making long-working-distance OCT probes.

The 2D scan in this OCT probe is realized by an electrothermal MEMS mirror with a footprint of 1.5 mm $\times$ 1.3 mm. Four pairs of bimorph actuators, which are symmetrically located at the four sides, are used to support and actuate the 0.5 mm $\times$ 0.5 mm aluminum-coated mirror plate, as illustrated in Fig. 3(a). Each bimorph actuator consists of three pairs of double S-shaped Al/SiO2 bimorph beams [32], [34]. A thin layer of Ti/TiN is embedded along all the bimorphs to form a heater in each of the bimorph actuators to drive the four bimorph actuators individually or collectively. The MEMS mirror is fabricated using a combined surface and bulk micromachining process similar to the one reported in [32]. This electro-thermal MEMS mirror generates an optical scan angle of $\pm$17.5° at only 5 volts. An SEM picture of the MEMS mirror is shown in Fig. 3(b). The resonant frequency of the MEMS mirror is 1.3 kHz. In our research, the fast axis scan is 200 Hz and the slow axis scan can be set as 0.4 Hz and 0.8 Hz.

3. Experimental Setup and Results

The optical model of the probe design is shown in Fig. 4(a), where d_1 is the distance from the C-lens rear end to the MEMS mirror plate and d_2 is the distance from the MEMS mirror to the beam waist. Considering the size and orientation of the MEMS chip as well as the machining precision and alignment process, d_1 is chosen as 2 mm, and thus $d_2 = 10$ mm. With the MEMS mirror scanning $\pm$17.5° optically, the target imaging area can reach up to 6.3 mm $\times$ 6.3 mm.

The MEMS chip is bonded on a flexible printed circuit board (FPCB) and then fixed on a titled 45° pedestal, as shown in Fig. 4(b). A zoomed-in view of the MEMS probe head is shown in Fig. 4(c). The outer diameter of the probe is 2.5 mm and the length of the rigid part is 8.5 mm. The MEMS device is driven by a 0-5 V triangular waveform voltage and the scan line at the beam waist position is about 6 mm long, as shown in Fig. 4(d).

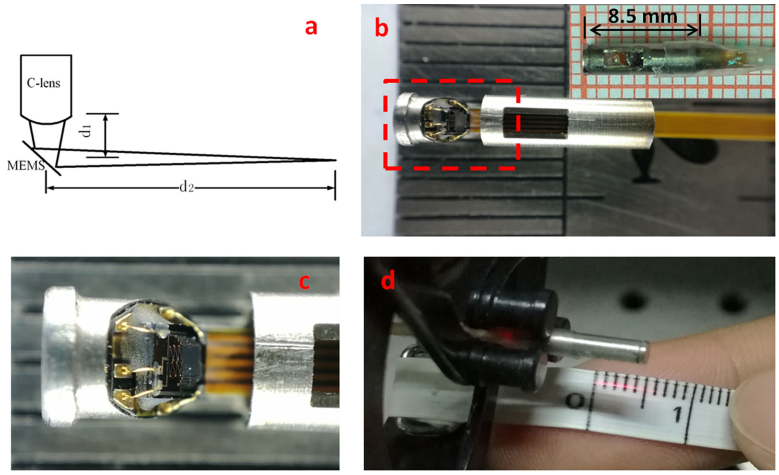

Fig. 4. (a) Optical model of the MEMS probe. (b) A photo of the MEMS probe with the MEMS chip bonded on a flexible PCB. (c) Zoom-in photo of the MEMS probe head. (d) The scan range of the MEMS probe.

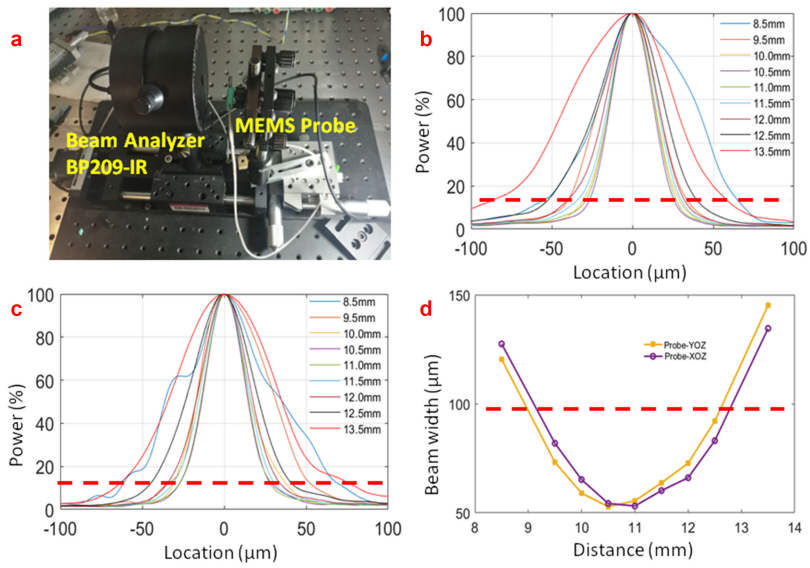

Fig. 5. (a) The beam quality testing setup. (b) The XOZ profile of the beam. (c) The YOZ profile of the beam. (d) The beam diameter changing along the propagation direction.

The quality of the optical beam coming out of the MEMS probe is tested with a beam analyzer (Thorlabs, BP209-IR). The test setup is shown in Fig. 5(a). The XOZ and YOZ profiles of the beam at various distances from the C-lens rear end are plotted in Figs. 5(b) and (c), respectively. The e^{-2} of the peak power is set as the cutoff for defining the beam diameter based on the Gaussian beam theory, which is marked with a red dotted line in Figs. 5(b) and 5(c). Then the beam widths at different distances are extracted from Figs. 5(b) and 5(c). The result is shown in Fig. 5(d), indicating that the beam waist is located at 11 mm and the diameter of the waist is about 50 μm. Also shown in Fig. 5(d), the distance range for the focused beam with the beam width less than 100 μm is about 3.4 mm, which is the depth of focus (DOF). This result is similar to that obtained using GRIN lens-based probes ($\sim$40 μm spot diameter and $\sim$10 mm working distance) [23], [24].

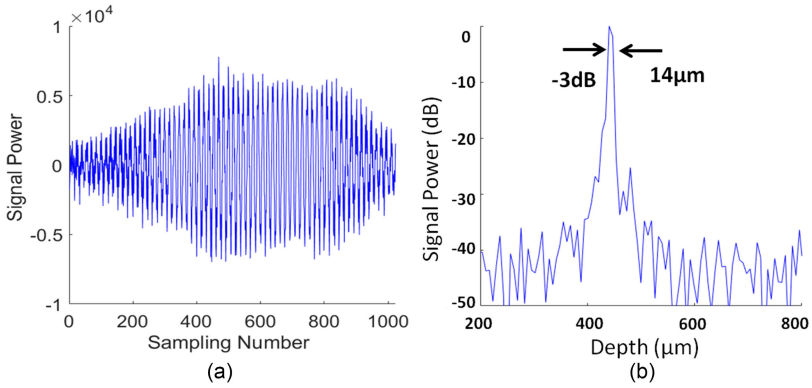

Fig. 6. (a): the original signal of the mirror. (b) The A-scan image

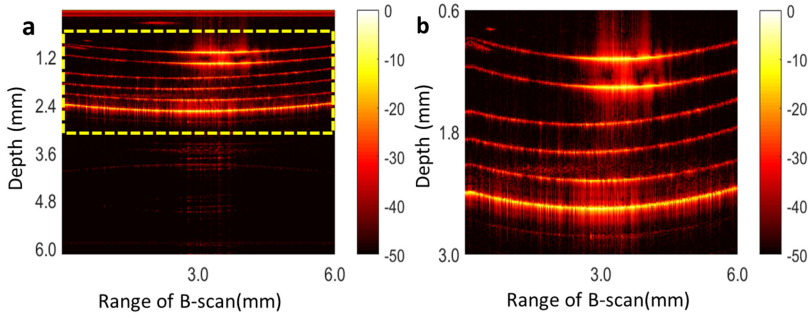

Fig. 7. (a) An OCT image of a 3-layer coverslip sample with a 6 mm imaging depth. (b) A portion of the image in (a) showing the imaging depth from 0.5 mm to 3.0 mm to highlight the OCT images of the coverslips.

This long-working distance probe is developed to provide large FOV for applications in organs with large surface areas such as stomach and bladder. For a short-working-distance OCT probe, the probe is often positioned against the surface of the tissue of examination while for the long-working distance probe reported here, it must be carefully considered how to position the probe properly to maintain and stabilize the working distance. One solution is to design a hollow accessory structure and assemble it at the tip of the probe as a spacer. Note that this probe is not intended for circumferential scanning in tubular organs. Instead, it can be used in tubular organs for more detailed imaging of suspicious regions that have been identified by other means.

The MEMS probe is connected to a swept source OCT system with a Santec swept source (Santec Technologies, HSL-20-100-B), and the interferometer system including a balanced photodetector is from Thorlabs (INT-MSI-1300B). The A-scan speed is determined by the sweeping speed of the swept source, which is 100 kHz. A mirror covered with gold film is used to test the axial resolution of our OCT system. The original signal at one point on the mirror is shown in Fig. 6(a) and the point spreading function (PSF) is shown in Fig. 6(b). The full width at -3 dB corresponds to the axial resolution of 14 μm. An optical filter (OD2) is placed in optical path to prevent overexposure of the balanced photodetector. The SNR of the OCT system is about 80 dB.

The OCT system was used to image a three-layer coverslip sample with 170–200 μm air gaps between the layers. As shown in Fig. 7, both the top and bottom surface of each coverslip returned reflection signals, so there are six bright lines in the OCT image. Note that the flat surfaces appear curved and this image deformation results from the radial scan of the MEMS mirror that forms spherical, fan-shaped and keystone distortions, and it can be corrected by an image-reverse method [33]. The subsequent images, as shown in Figs. 8 and 9, are corrected by the image-reverse method. It is also worthy to notice that the OCT image area is as wide as 6 mm, which at least more than

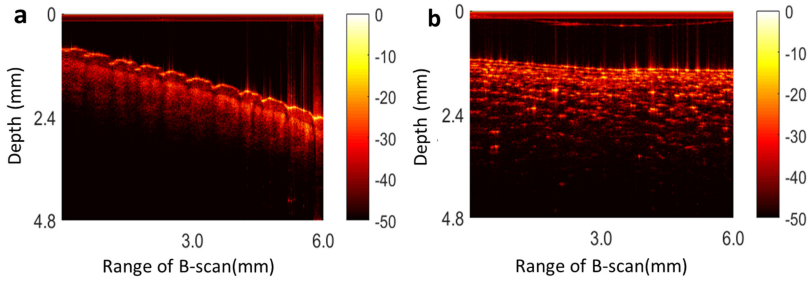

Fig. 8. (a) OCT image of human finger. (b) OCT image of onion.

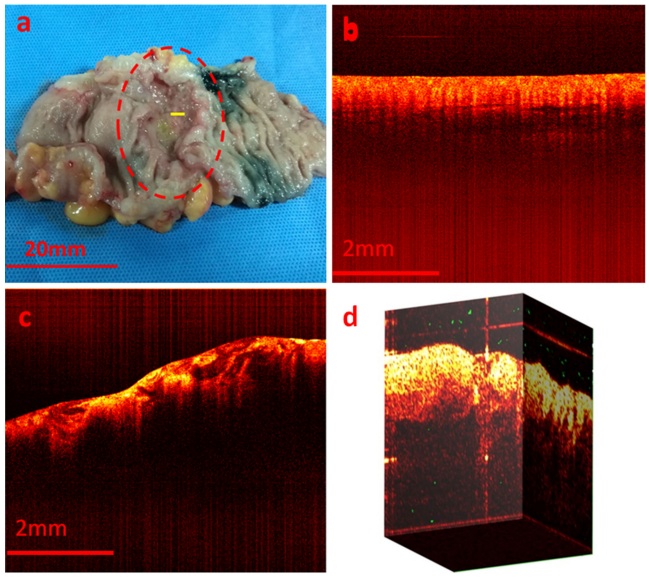

Fig. 9. (a) A freshly excised cancerous colon sample. (b) OCT image of normal tissue. (c) OCT image of cancerous tissue. (d) The 3D image of the cancerous tissue.

twice as much as those obtained from previous MEMS OCT probes [9], [11], [12], [13], [15], [32]. Human finger and onion were imaged using the MEMS OCT probe; the corresponding OCT images are shown in Fig. 8(a) and (b).

Fig. 9(a) shows a cancerous colon sample with the cancerous tissue area of about 20 mm $\times$ 40 mm marked by a red dash line. The OCT images of the normal tissue and the cancerous tissue are shown in Fig. 9(b) and Fig. 9(c), respectively. In general, a normal colon tissue has a layered structure and each layer is homogeneous, so the intensity at the same depth in an OCT image is approximately the same. In contrast, a cancerous tissue does not have an obvious layered structure or even has no layers at all. The OCT image with a 6 mm-wide range in Fig. 9(c) presents the various characteristics of the cancerous tissue very well. As a comparison, if an OCT image with only a 2 mm range were obtained, it would be much more difficult to determine the cancerous characteristics. A 3D OCT image of the cancerous tissue has also been reconstructed, as shown in Fig. 9(d).

4. Conclusions

In summary we have successfully demonstrated a 2.5 mm-diameter miniature endoscopic OCT probe based on a C-lens. The length tolerance of machining C-lenses is 10–20 times more than

that of machining GRIN lenses. Thus, C-lenses are a better choice for making long-working-distance OCT probes. The new OCT probe design using a C-lens results in a considerably longer working distance of 12 mm and a large imaging area of 6 mm $\times$ 6 mm. The lateral resolution is 50 μm, which is comparable to other circumferential scanning OCT used clinically in artery and esophagus. In addition, the lateral resolution of 50 μm is also comparable to those obtained with GRIN lens-based probes [24]. And the lateral resolution can be improved by increasing the C-lens diameter and the size of the MEMS mirror, i.e., increasing the NA of the imaging system. This probe can scan the targeted area of interest without pulling or pushing or rotating the probe. Thus more stable scans and higher quality OCT images can be obtained. The outer diameter of 2.5 mm is another advantage since the probe can be directly inserted through the biopsy channel of a variety of conventional endoscopes. This work is focusing on demonstrating the feasibility of C-lenses for long working distance. Our following study needs needs more clinical study in detecting dysplastic lesions. This MEMS OCT probe with much increased imaging area has great potential for in vivo endoscopic diagnosis and intraoperative imaging.

References

[1] M. J. Gora, M. J. Suter, G. J. Tearney, and X. Li., "Endoscopic optical coherence tomography: Technologies and clinical applications [Invited]," *Biomed. Opt. Express*, vol. 8, no. 5, pp. 2444–2484, 2017.

[2] G. J. Tearney *et al.*, "In vivo endoscopic optical biopsy with optical coherence tomography," *Science*, vol. 276, pp. 2037–2039, 1997.

[3] M. V. Sivak *et al.*, "High-resolution endoscopic imaging of the GI tract using optical coherence tomography," *Gastrointestinal Endosc.*, vol. 51, pp. 474–479, 2000.

[4] S. Jackle *et al.*, "In vivo endoscopic OCT of esophagitis, Barrett's esophagus, and adenocarcinoma of the esophagus," *Endoscopy*, vol. 32, pp. 750–755, 2000.

[5] Y. Wang, M. Bachman, G. P. Li, S. Guo, B. J. F. Wong, and Z. Chen, "Low-voltage polymer-based scanning cantilever for in vivo optical coherence tomography," *Opt. Lett.*, vol. 30, pp. 53–55, 2005.

[6] P. R. Herz, Y. Chen, A. D. Aguirre, J. G. Fujimoto, H. Mashimo, and J. Schmitt, "Ultrahigh resolution optical biopsy with endoscopic optical coherence tomography," *Opt. Express*, vol. 12, no. 15, pp. 3532–3542, 2004.

[7] P. H. Tran, D. S. Mukai, M. Brenner, and Z. P. Chen, "In vivo endoscopic optical coherence tomography by use of a rotational microelectromechanical system probe," *Opt. Lett.*, vol. 29, pp. 1236–1238, 2004.

[8] N. Zhang *et al.*, "Compact piezoelectric transducer fiber scanning probe for optical coherence tomography," *Opt. Lett.*, vol. 39, no. 2, pp. 186–188, 2014.

[9] L. Liu, L. Wu, J. J. Sun, E. Lin, and H. K. Xie, "Miniature endoscopic optical coherence tomography probe employing a two-axis microelectromechanical scanning mirror with through-silicon vias," *J. Biomed. Opt.*, vol. 16, no. 2, 2011.

[10] A. Jain, A. Kopa, Y. T. Pan, G. K. Fedder, and H. K. Xie, "A two-axis electrothermal micromirror for endoscopic optical coherence tomography," *IEEE J. Sel. Topics Quantum Electron.*, vol. 10, no. 3, pp. 636–642, May/Jun. 2004.

[11] W. G. Jung *et al.*, "In vivo three-dimensional spectral domain endoscopic optical coherence tomography using a microelectromechanical system mirror," *Opt. Lett.*, vol. 32, no. 22, pp. 3239–3241, 2007.

[12] J. Sun *et al.*, "3D in vivo optical coherence tomography based on a low voltage, large-scan-range 2D MEMS mirror," *Opt. Express*, vol. 18, pp. 12065–12075, 2010.

[13] K. H. Kim *et al.*, "Two-axis magnetically-driven MEMS scanning catheter for endoscopic high-speed optical coherence tomography," *Opt. Express*, vol. 15, pp. 18130–18140, 2007.

[14] D. L. Wang *et al.*, "Endoscopic swept-source optical coherence tomography based on a two-axis microelectromechanical system mirror," *J. Biomed. Opt.*, vol. 18, no. 8, 2013.

[15] C. Duan, Q. Tanguy, A. Pozzi, and H. K. Xie, "Optical coherence tomography endoscopic probe based on a tilted MEMS mirror," *Biomed. Opt. Express*, vol. 7, no. 9, pp. 3344–3353, 2016.

[16] Nine Point Company, Bedford, MA, USA. [Online]. Available: http://www.ninepointmedical.com/nvisionvle-imaging-system

[17] C. Zhou *et al.*, "Three-dimensional endoscopic optical coherence tomography imaging of cervical inlet patch," *Gastrointestinal Endosc.*, vol. 75, no. 3, pp. 675–677, 2012.

[18] J. Ortiz-Fernandez-Sordo, A. Parra-Blanco, and A. Garcia-Varona, "Endoscopic resection techniques and ablative therapies for Barrett's neoplasia," *World J. Gastrointestinal Endosc.*, vol. 3, no. 9, pp. 171–182, 2011.

[19] T. H. Tsai, J. G. Fujimoto, and H. Mashimo, "Endoscopic optical coherence tomography for clinical gastroenterology," *Diagnostics, Basel*, vol. 4, no. 2, pp. 57–93, 2014.

[20] T. S. Kirtane and M. S. Wagh, "Endoscopic optical coherence tomography (OCT): Advances in gastrointestinal imaging," *Gastroenterol. Res. Pract.*, vol. 2014, 2014, Art. no. 376367.

[21] C. Duan, J. J. Sun, S. Samuelson, and H. K. Xie, "Probe alignment and design issues of microelectromechanical system based optical coherence tomography endoscopic imaging," *Appl. Opt.*, vol. 52, no. 26, pp. 6589–6598, 2013.

[22] M. J. Suter *et al.*, "Comprehensive microscopy of the esophagus in human patients with optical frequency domain imaging," *Gastrointestinal Endosc.*, vol. 68, no. 4, pp. 745–753, 2008.

[23] W. Kang *et al.*, "Endoscopically guided spectral-domain OCT with double-balloon catheters," *Opt Express*, vol. 18, no. 16, pp. 17364–17372, 2010.

[24] H. L. Fu, Y. X. Leng, M. J. Cobb, K. Hsu, J. H. Hwang, and X. D. Li, "Flexible miniature compound lens design for high-resolution optical coherence tomography balloon imaging catheter," *J Biomed. Opt.*, vol. 13, no. 6, 2008.
[25] J. F. Xi, L. Huo, Y. C. Wu, M. J. Cobb, J. H. Hwang, and X. D. Li, "High-resolution OCT balloon imaging catheter with astigmatism correction," *Opt. Lett.*, vol. 34, no. 13, pp. 1943–1945, 2009.
[26] T. S. Wang, A. F. W. van der Steen, and G. van Soest, "Numerical analysis of astigmatism correction in gradient refractive index lens based optical coherence tomography catheters," *Appl. Opt.*, vol. 51, no. 21, pp. 5244–5252, 2012.
[27] W. Jung, W. Benalcazar, A. Ahmad, U. Sharma, H. Tu, and S. A. Boppart, "Numerical analysis of gradient index lens-based optical coherence tomography imaging probes," *J. Biomed. Opt.*, vol. 15, no. 6, 2010.
[28] W. C. Jing *et al.*, "Design and implementation of a broadband optical rotary joint using C-lenses," *Opt. Express*, vol. 12, no. 17, pp. 4088–4093, 2004.
[29] CASIX Co., Ltd., Fujian, China. *Collimators: C-Lens*. [Online]. Available: http://www.casix.com/products/fiber-optics-subs/collimators.shtml
[30] S-q. Wang, Y. Ruan, D.-L. Yin, and Z.-W. Yang, "The calculation and analyzing of the RL of C-lens collimator," (in Chinese), *Optoelectron. Technol. Inf.*, vol. 16, no. 1, pp. 24–28, 2003.
[31] Femto Optics Tech. Co., Ltd., Xi'an, China. [Online]. Available: http://www.feteco.com/about/37.html
[32] S. R. Samuelson, L. Wu, J. J. Sun, S. W. Choe, B. S. Sorg, and H. K. Xie, "A 2.8-mm Imaging probe based on a high-fill-factor MEMS mirror and wire-bonding-free packaging for endoscopic optical coherence tomography," *J. Microelectromech. Syst.*, vol. 21, no. 6, pp. 1291–1302, 2012.
[33] D. L. Wang, P. Liang, S. Samuelson, H. Z. Jia, J. S. Ma, and H. K. Xie, "Correction of image distortions in endoscopic optical coherence tomography based on two-axis scanning MEMS mirrors," *Biomed. Opt. Express*, vol. 4, no. 10, pp. 2066–2077, 2013.
[34] S. R. Samuelson and H. Xie, "A large piston displacement MEMS mirror with electrothermal ladder actuator arrays for ultra-low tilt applications," *J. Microelectromech. Syst.*, vol. 23, no. 1, pp. 39–49, 2014.